LAWRENCE
LIVERMORE
NATIONAL
LABORATORY

LLNL-TR-408299

Generalized Subtraction Schemes for the Difference Formulation in Radiation Transport

T. Luu, E. Brooks, A. Szoke

October 30, 2008

Disclaimer

This work performed under the auspices of the U.S. Department of Energy by Lawrence Livermore National Laboratory under Contract DE-AC52-07NA27344.

Generalized Subtraction Schemes for the Difference Formulation in Radiation Transport ⋆

Thomas Luu *, Eugene D. Brooks III, Abraham Szőke

Lawrence Livermore National Laboratory
P.O. Box 808, Livermore, CA 94550, USA

Abstract

In the difference formulation for the transport of thermally emitted photons, the photon intensity is defined relative to a reference field, the black body at the local material temperature. This choice of reference field removes the cancellation between thermal emission and absorption that is responsible for noise in the Monte Carlo solution of thick systems, but introduces time and space derivative source terms that can not be determined until the end of the time step. It can also lead to noise induced crashes under certain conditions where the real physical photon intensity differs strongly from a black body at the local material temperature.

In this report, we consider a difference formulation relative to the material temperature at the beginning of the time step, and in the situations where the radiation intensity more closely follows a temperature other than the local material temperature, that temperature. The result is a method where iterative solution of the material energy equation is efficient and noise induced crashes are avoided. To support our contention that the resulting generalized subtraction scheme is robust, and therefore suitable for practical use, we perform a stability analysis in the thick limit where instabilities usually occur.

Key words: difference formulation, radiation transport, implicit Monte Carlo

⋆ This work performed under the auspices of the U.S. Department of Energy by Lawrence Livermore National Laboratory under Contract DE-AC52-07NA27344.
* Corresponding Author:
Email address: luu5@llnl.gov (Thomas Luu).

1 Introduction

Radiation transport in media is described by the Boltzmann equation for photons coupled to the material energy equation, which in slab geometry under the assumptions of no scattering, no material motion, and local thermodynamic equilibrium (LTE) for the material is given by

$$\left(\frac{1}{c}\frac{\partial}{\partial t} + \mu\frac{\partial}{\partial x} + \sigma\right) I = \sigma B \quad , \tag{1}$$

$$\frac{\partial E_{mat}}{\partial t} = 2\pi \int d\nu d\mu \; \sigma(I - B) \quad . \tag{2}$$

Here I represents the intensity field, $1/\sigma$ the absorption length for photons, E_{mat} the energy density of the material, ν the frequency, μ the direction cosine of photon travel, and B the blackbody field at the material temperature given by

$$B = \frac{2h\nu^3}{c^2}\frac{1}{e^{h\nu/kT_{mat}} - 1} \quad . \tag{3}$$

The black body emission function, Eq. (3), can be expressed in terms of a "reduced" frequency distribution function, $b(\nu, T)$,

$$B(\nu, T) = \frac{caT^4}{4\pi} b(\nu, T) \quad , \tag{4}$$

where a is the radiation constant. The advantages of using the reduced frequency distribution function are that the strong temperature dependence of thermal emission is factored out by the T^4 term, and that its frequency integral is independent of temperature,

$$\int_0^\infty d\nu \, b(\nu, T) = 1 \quad . \tag{5}$$

There is an extensive collection of numerical algorithms that have been developed for solving the coupled equations above after discretization in space and time (see [1] and references within for a review of existing algorithms). Of recent interest are transport algorithms that obtain the correct diffusion limit in the appropriate regime [2–5]. The particular discretizations employed in these algorithms provide accurate solutions as the physical system approaches the diffusion limit, without having to shrink the zone sizes to scales smaller than the photon mean free path, $1/\sigma$, or the time steps shorter than the mean free time, $1/\sigma c$, of a photon, as long as variations in the material physical properties are resolved.

The difference formulation employed in [5–8] defined the difference field as $D = I - B$, where B is the black-body radiation field at the material temperature at each point in space and time, with the exception of special treatment

of boundary conditions that reduced Monte Carlo noise. In terms of the difference field, D, Eqs. (1) and (2) become

$$\left(\frac{1}{c}\frac{\partial}{\partial t}+\mu\frac{\partial}{\partial x}+\sigma\right)D=-\left(\frac{1}{c}\frac{\partial}{\partial t}+\mu\frac{\partial}{\partial x}\right)B \quad , \tag{6}$$

$$\frac{\partial E_{mat}}{\partial t}=2\pi\int d\nu d\mu\ \sigma D \quad . \tag{7}$$

Note that in this formulation, the original σB source of Eq. (1) is replaced with derivative sources

$$-\left(\frac{1}{c}\frac{\partial}{\partial t}+\mu\frac{\partial}{\partial x}\right)B \quad . \tag{8}$$

The vices and virtues of this particular transformation are discussed in detail in [6,7].

The difference formulation is not restricted to using the black body field corresponding to the local material temperature, B, as the reference field. Any choice for the reference field, $\overline{B}$, may be used and the resulting formulation of the transport equation will still be rigorously equivalent to the original one. If the black body corresponding to the material temperature is used, the Monte Carlo noise arising from the near cancellation of thermal emission and absorption, $\sigma(I-B)$ in Eq. (2), that occurs in optically thick regions is removed. Alternative choices for the reference field might sacrifice some of the advantage gained by completely removing this term in order to gain an advantage with respect to other sources of noise in a Monte Carlo implementation of the transport algorithm [9].

In this report, we consider several generalizations of the difference formulation that pose a significant advantage for practical problems. The difference formulation is generalized by defining $D=I-\overline{B}$ where $\overline{B}$ is the black body function at some judiciously chosen temperature. In this case the transport and energy equations become

$$\left(\frac{1}{c}\frac{\partial}{\partial t}+\mu\frac{\partial}{\partial x}+\sigma\right)D=\sigma(B-\overline{B})-\left(\frac{1}{c}\frac{\partial}{\partial t}+\mu\frac{\partial}{\partial x}\right)\overline{B} \quad , \tag{9}$$

$$\frac{\partial E_{mat}}{\partial t}=2\pi\int d\nu d\mu\ \sigma D-2\pi\int d\nu d\mu\ \sigma(B-\overline{B}) \quad . \tag{10}$$

Obviously, if $\overline{B}=B$ one recovers Eqs. (6) and (7). When $\overline{B}=0$, one recovers Eqs. (1) and (2).

There are several motivations for using a generalization of the difference formulation. If $\overline{B}$ is known at the beginning of the time step, the derivative

sources in Eq (9),

$$-\left(\frac{1}{c}\frac{\partial}{\partial t}+\mu\frac{\partial}{\partial x}\right)\overline{B} \quad , \tag{11}$$

are themselves known. This makes these sources easier to sample in complicated geometries, reduces the cost of scoring the particles, and reduces the complexity of the nonlinear system that represents the energy equation. In this case, the only source that contains unknown factors is the remainder source

$$\sigma(B-\overline{B}) \quad , \tag{12}$$

which, aside from any complicated frequency dependence of σ, is relatively simple to sample as it is isotropic. If $\overline{B}$ is the value of B at the beginning of the time step and the problem is slowly varying, the unknown remainder source term, $\sigma(B-\overline{B})$, is small and can be handled as a perturbation on the otherwise explicit solution for the transport equation, making it amenable to iterative solution techniques. In particular, we have found a solution strategy that involves no matrix inversions, and only a very few matrix multiplications. We demonstrate the solution efficiency, accuracy, and stability for this technique in this paper.

Another motivation for a generalized difference formulation comes from the fact that there can be regions of a problem where the radiation temperature that corresponds to the radiation energy density is not close to the material temperature. If the radiation and the material temperatures differ by a significant amount a Monte Carlo solution of Eqs. (6) and (7) will be intrinsically noisy due to the large difference field. Such a scenario can occur, for example, in problems that have both optically thick and thin regions that have significantly different material temperatures. Because of weak coupling between the radiation and material in the optically thin regions, the radiation temperature in these regions is dominated by the material temperature in the adjacent optically thick regions. Thus within the optically thin regions, a choice for $\overline{B}$ that tracks the material temperature of the adjacent optically thick regions produces a small difference field, D, and therefore lowers Monte Carlo noise. In this paper, we will show a specific example of such a scenario and how this modification to the reference field makes a significant improvement.

We perform stability analyses of the original difference formulation, and the modified schemes presented in this paper, in the thick limit. In doing so we derive stability criteria that enable us to accurately predict the failure of our algorithms, where it occurs. In addition to being illuminating, these analyses give confirmation of our experience with the robustness of the computational methods we describe in this report.

The report is organized in the following manner: Section 2 explains our discretization schemes and describes our method of solving the equation for the material energy. Where pertinent, it gives sample calculations that help to

show the differences between the original difference formulation and the generalized subtraction method described here. Section 3 gives specific examples that show the superiority of this new method when compared to the original difference formulation. Section 4 describes our stability analysis. We conclude in Section 5.

2 Discretization scheme and Monte Carlo energy weights

In order to solve the time dependent transport problem posed in Eqs. (9) and (10), with suitable boundary conditions, the problem domain is divided into N zones, enumerated by $1 \leq i < N$, and the transport equation is "solved" by working out the total energy of the source terms and emitting it as Monte Carlo particles with appropriate coordinate distributions. Each Monte Carlo particle carries an energy weight that decays exponentially as it travels, losing energy to the material. The change in the material energy for the time step, from t_0 to $t_0 + \Delta t$, is accounted for in each zone by evaluating the integrals in Eq. (10) over the time step, in each zone. These integrals are evaluated by scoring Monte Carlo particles, track by track, along with deterministic integrals that arise due to the fact that a $\overline{B}$ has been chosen that does not completely cancel the thermal emission term, σB.

Stability of the time dependent solution requires implicit treatment of the source terms, leading to some Monte Carlo particles with energy weights that will not be known until the end of the time step. The Symbolic Implicit Monte Carlo method [10] is used to account for the energy depositions from particles with energy weights that will not be known until the end of the time step. The energy equation, Eq. (10), becomes a nonlinear matrix equation in this scheme. The solution of this matrix equation provides the material temperatures for the end of the time step.

For the results shown in the paper, we use the interpolation method described in [5], interpolating $\overline{B}$ between zone centers only for the space derivative source term of Eq. (11). This spreads between the zone centers what would be a Dirac delta function source at the interface between zones and provides the correct flux between zones in steady state, in the diffusion limit. For brevity, we will not repeat the detailed description of the interpolation method here. The only modification is the simplification that the derivative sources are known, simplifying sampling and scoring. The isotropic source term, $\sigma(B - \overline{B})$, is the only term with unknown particle energy weights. We will discuss how this source term is sampled in what follows.

The Monte Carlo particles that are tracked through the time step, t_0 to $t_0+\Delta t$, are composed of the census particles from the prior time step, particles that

are born during the time step due to the source terms given by Eqs. (11) and (12), and any source terms that arise from the boundary conditions for the problem. As has become well known for implicit Monte Carlo transport of thermally generated photons, and will be explored for a specific situation in detail later in this paper, we need to use the unknown end of time step value for B in our source terms if we are to obtain stable time dependent behavior.

2.1 Specific example of $\overline{B} = B(t_0)$

As an example of a known reference field, and its consequences on the energy weights of Monte Carlo particles, consider the following expression for $\overline{B}$,

$$\overline{B}(t) = B(t_0) \qquad (t_0 \leq t < t_0 + \Delta t) \quad . \tag{13}$$

Here $\overline{B}$ is a series of step functions in time; its value for the duration of the time step, from t_0 to $t_0 + \Delta t$, being the known value of B determined at the end of the prior time step. By using $B(t_0)$ for $\overline{B}$ during the time step, the source terms given by Eq. (11) are known, and as such do not contribute to off-diagonal terms in the nonlinear system that must be solved in order to resolve the change in material energy at the end of the time step.

With this definition of $\overline{B}$, the frequency dependence of the explicit sources in Eq. (11) can be factored out in the following manner,

$$\left(\frac{1}{c}\frac{\partial}{\partial t} + \mu\frac{\partial}{\partial x}\right)\overline{B} = \frac{4\pi}{c}\frac{\partial\overline{B}}{\partial\overline{\Phi}}\left(\frac{1}{4\pi}\frac{\partial\overline{\Phi}}{\partial t} + \frac{\mu c}{4\pi}\frac{\partial\overline{\Phi}}{\partial x}\right) \quad . \tag{14}$$

Here $\overline{\Phi}(t) = aT^4(t_0)$, $(t_0 \leq t < t_0 + \Delta t)$, and $\partial\overline{B}/\partial\overline{\Phi}$ represents a frequency distribution since it is positive and satisfies [8]

$$\frac{4\pi}{c}\int_0^\infty d\nu\ \frac{\partial\overline{B}}{\partial\overline{\Phi}} = 1 \quad . \tag{15}$$

Efficient techniques have been developed for frequency sampling the integrand in Eq. (15) [8]. We now continue our derivation of our Monte Carlo energy weights using this definition of $\overline{B}$. In later sections, we will give other examples of Eq. (13) (though really just slight modifications of Eq. (13)) and where necessary, will show how the derivations below are altered.

2.2 Monte Carlo sources

With the definition of $\overline{B}$ given by Eq. (13), and our discretization scheme laid out, we can now evaluate the energy weight of the isotropic remainder source.

During the time interval from t_0 to $t_0 + \Delta t$, this source is given by

$$\sigma(B_i - \overline{B}_i) = \sigma \frac{4\pi}{c} \frac{\partial B}{\partial \Phi} \left[\frac{c}{4\pi} (\Phi_i(t_0 + \Delta t) - \Phi_i(t_0)) \right] \quad , \tag{16}$$

where the subscript, i, is the zone index and we are assuming small changes in Φ. (There are situations, such as the reference field choice of Section 3.2.3, where the difference in Φ for the remainder source term is large. These require the use of a finite difference approach for the construction of the frequency distribution.) Integrating this within zone i, across the time step from t_0 to $t_0 + \Delta t$, over the range of direction cosines, and over all frequencies, the total energy weight associated with this source is given by

$$\int_{x_i}^{x_{i+1}} dx \int_{t_0}^{t_0+\Delta t} dt \int_{-1}^{1} d\mu \int d\nu \, \sigma(B - \overline{B}) = \frac{c \, \Delta x \, \Delta t}{2\pi} \langle \sigma \rangle_i \left[\Phi_i(t_0 + \Delta t) - \Phi_i(t_0) \right] \quad , \tag{17}$$

where

$$\langle \sigma \rangle_i = \frac{4\pi}{c} \int d\nu \; \sigma \frac{\partial \overline{B}_i}{\partial \overline{\Phi}_i} \quad . \tag{18}$$

The frequency distribution of this source is given by

$$\frac{4\pi}{c} \sigma \frac{\partial \overline{B}_i}{\partial \overline{\Phi}_i} / \langle \sigma \rangle_i \quad . \tag{19}$$

Obviously, for gray opacities $\langle \sigma \rangle_i = \sigma$. The treatment of the material independent source terms, Eq. (14), is similar to the treatment found in [7,8], except that all of the source parameters are known in this case.

2.3 Newton-Raphson solution strategy for finding the material energy E_{mat}

The unknowns, $\Phi_i(t_0 + \Delta t)$, are calculated by solving the material energy equation, Eq. (10), at the end of the time step, $t_0 + \Delta t$. To accomplish this, we first formally integrate Eq. (10) from t_0 to $t_0 + \Delta t$ to obtain the following function,

$$\begin{aligned} f(x) = {} & E_{mat}(T(x, t_0)) - E_{mat}(T(x, t_0 + \Delta t)) \\ & + 2\pi \int_{t_0}^{t_0+\Delta t} dt \int d\nu \int d\mu \, \sigma(\nu, T(x, t_0)) D(x, t; \nu, \mu) \\ & + \int_{t_0}^{t_0+\Delta t} dt \; G(x, t) - 2\pi \int_{t_0}^{t_0+\Delta t} dt \int d\nu \int d\mu \, \sigma(B - \overline{B}) \quad . \end{aligned} \tag{20}$$

We then integrate $f(x)$ within each zone i, thereby defining the following quantities,

$$
\begin{aligned}
f_i &= \int_{x_i}^{x_{i+1}} dx f(x) \quad , \\
&= E_i(t_0) - E_i(t_0 + \Delta t) + (\sigma D)_i + G_i - (\sigma \Delta B)_i \quad , \qquad (21)
\end{aligned}
$$

where

$$
E_i = \int_{x_i}^{x_{i+1}} dx\, E_{mat}(T) = \Delta x_i \frac{\rho c_\nu}{a^{1/4}}\, \Phi_i^{1/4} \quad , \qquad (22)
$$

$$
G_i = \int_{x_i}^{x_{i+1}} dx\, G(x) \quad , \qquad (23)
$$

$$
\begin{aligned}
(\sigma \Delta B)_i &= 2\pi \int_{x_i}^{x_{i+1}} dx \int_{t_0}^{t_0+\Delta t} dt \int d\nu \int d\mu\ \sigma(B - \overline{B}) \\
&= \quad c \langle \sigma \rangle_i \Delta x\ \Delta t \left[\Phi_i(t_0 + \Delta t) - \Phi_i(t_0) \right] \quad , \qquad (24)
\end{aligned}
$$

and

$$
\begin{aligned}
(\sigma D)_i &= 2\pi \int_{x_i}^{x_{i+1}} dx \int_{t_0}^{t_0+\Delta t} dt \int d\nu \int d\mu\, \sigma(\nu, T(x,t_0)) D(x,t;\nu,\mu) \\
&= N_i \\
&+ \sum_j (REM)_i^j\ (\Phi_j(t_0 + \Delta t) - \Phi_j(t_0)) \\
&+ \sum_j (DDT)_i^j\ (\Phi_j(t_0) - \Phi_j(t_0 - \Delta t)) \\
&+ \sum_j (DDX)_i^j\ (\Phi_{j-1}(t_0) - \Phi_j(t_0)) \quad . \qquad (25)
\end{aligned}
$$

We have assumed that ρC_v is constant within each zone, during the time step. N_i is the contribution from the census particles to zone i from the prior time step, $(REM)_i^j$ is the contribution to zone i due to remainder sources, $\sigma(B_j - \overline{B}_j)$, emanating from zone j, $(DDT)_i^j$ is the contribution to zone i from the time-derivative sources emanating from zone j, and $(DDX)_i^j$ is the contribution to zone i from gradient sources from zone j. The dependence of the time derivative sources on $\Phi(t_0 - \Delta t)$ arises from that fact that the reference field is adjusted at the beginning of the time step. Note the nonlinearity of Φ in Eq. (22). Our unknown $\Phi_j(t_0 + \Delta t)$ are found by demanding that $f_i = 0$ for all i. We solve for these by way of a Newton-Raphson iteration algorithm.

We note that of all the terms appearing in Eq. (21), only the portion of $(\sigma D)_i$ due to remainder sources carries a dependence on the unknown $\Phi_j(t_0 + \Delta t)$ for spatial zones $j \neq i$.

2.4 Alternative iterative solution strategy for finding the material energy E_{mat}

The Newton-Raphson procedure described above converges quickly but requires the solution of a linear system for the error at each step. The cost of solving the linear system scales poorly as the number of zones in the problem is increased. In order to address this problem, we have developed an alternative iterative solution strategy that is a variant of Jacobi iteration. We provide a synopsis of Jacobi iteration here and then show how to solve the nonlinear material energy equation using a similar strategy.

Assuming that one wants the solution to

$$A\,x = b \quad , \tag{26}$$

one decomposes the matrix A into $A = D + L + U$, where D is a diagonal matrix, L is lower triangular and U is upper triangular. Rewriting, one obtains

$$D\,x = [b - (L + U)x] \quad . \tag{27}$$

If all of the diagonal matrix elements are nonzero, Eq. (27) can be used as a prescription for iterating a solution,

$$x^{k+1} = D^{-1}[b - (L + U)x^k] \quad . \tag{28}$$

If the original matrix, A, is diagonally dominant this iterative process, known as Jacobi iteration, converges.

Examining Eqs. (21) through (25), we see that Eq. (21) can be put in the form

$$NL\,(x^{1/4}) + A\,x = b \quad , \tag{29}$$

where x is a vector of the unknowns, $\Phi_j(t_0+\Delta t)$, $(x^{1/4})$ is a vector of $\Phi_j^{1/4}(t_0 + \Delta t)$, NL is a diagonal matrix and A can be decomposed into $A = D + L + U$. Rewriting, and casting into a form similar to the case for Jacobi iteration, we obtain

$$NL\,(x^{1/4})^{k+1} + D\,x^{k+1} = b - (L + U)\,x^k \quad . \tag{30}$$

The left hand side is not a linear operator, so the refined solution is not obtained by simple division. A particular root of a quartic equation, however, produces each element of x^{k+1}.

At the cost of a reduced rate of convergence, compared to Newton-Raphson iteration, the solution of a linear system has been traded for a matrix-vector multiply. The method can be extended to handle real material specific heats that are functions of temperature. One could also explore similar nonlinear

extensions of iterative linear system solvers that provide faster convergence than Jacobi iteration.

3 Test Examples

We now give two examples that help show the improved efficacy of using a reference field $\overline{B}$ different from that of the original difference formulation. We show results where we have employed both the Newton-Raphson solution strategy and the alternative iterative solution strategy of the material energy equation.

When using the alternative iterative solution strategy, at each time step the iteration ends when our prescribed figure of merit,

$$\varepsilon = \sqrt{\sum_i \left(\frac{\Phi_i^{new} - \Phi_i^{old}}{\Phi_i^{old}} \right)^2} \quad , \tag{31}$$

is less then some pre-defined value. Here the sum is over all zones and the superscripts *new* and *old* refer to the current iterative value of Φ_i and the previous value of Φ_i, respectively.

3.1 Marshak wave example

As an example of the particular reference field $\overline{B}$ given in Eq. (13), we have run Marshak wave calculations using a gray $\sigma = 200$ cm^{-1}, $\rho\, C_v = .1$ jerk/cm^3 (1 jerk = 10^9 joules), and 80 equally spaced zones over a slab of length 5 cm, giving 12.5 mean free paths per zone. A time step size of 0.01 sh, 1 sh = 10^{-8} seconds, is used in these calculations. The temperature at the left edge of the problem is held at 1 keV and the temperature of the slab is initially zero. Figure 1 shows our results at various times, where we have performed our calculations using both the Newton-Raphson solution strategy (red) and alternative iterative solution strategy (green) described in the previous section. Our termination criterion for these runs is $\varepsilon \leq .01$. Also shown for comparison in black is the same problem using the original difference formulation (*i.e.* $\overline{B} = B(t_0 + \Delta t)$). Overall there is good agreement between the methods; the main discrepancy occurs only at early times. The difference here can be attributed to the fact that during the first time step of a run using the explicit reference field of Eq. (13), the spatial gradient is much larger than in a fully implicit treatment, leading to higher energy flow. Since the original difference formulation is fully implicit, the smaller spatial gradient at the end of the time step leads to a lower energy flow. This is apparent during the first few time

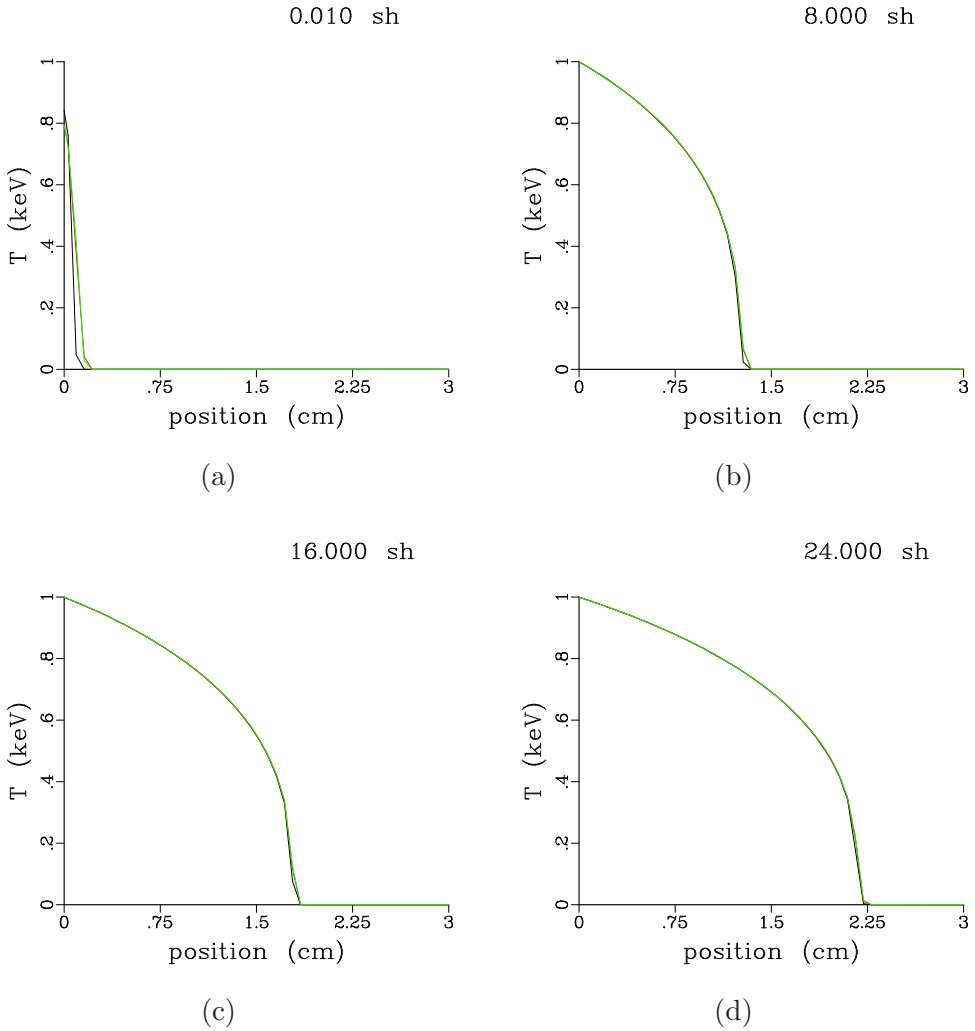

Fig. 1. Comparison of Marshak wave calculations at various times using $\overline{B} = B(t_0)$ with the Newton-Raphson solution strategy (red) and alternative iterative solution strategy (green) described in text. Also shown are results of the original difference formulation, using $\overline{B} = B(t_0 + \Delta t)$ (black).

steps, as shown in Fig. 1, but the discrepancy evaporates once the problem has run for a while. Suitable time step control removes this discrepancy.

In Fig. 2 (a) we show, as a function of time step, the number of iterations needed before our termination criterion is met for various values of ε. The range of time steps shown in Fig. 2 corresponds to the first 1/2 shake of the problem described in the previous paragraph. A remarkable feature born out in this figure is that, on average, the number of iterations for a given tolerance remains the same, even at early time steps when the Marshak wave is just penetrating the slab. In Fig. 2 (b) we plot the average number of iterations needed for convergence as a function of tolerance. Note the logarithmic scale used for the x-axis. The apparent linear behavior suggests power-law conver-

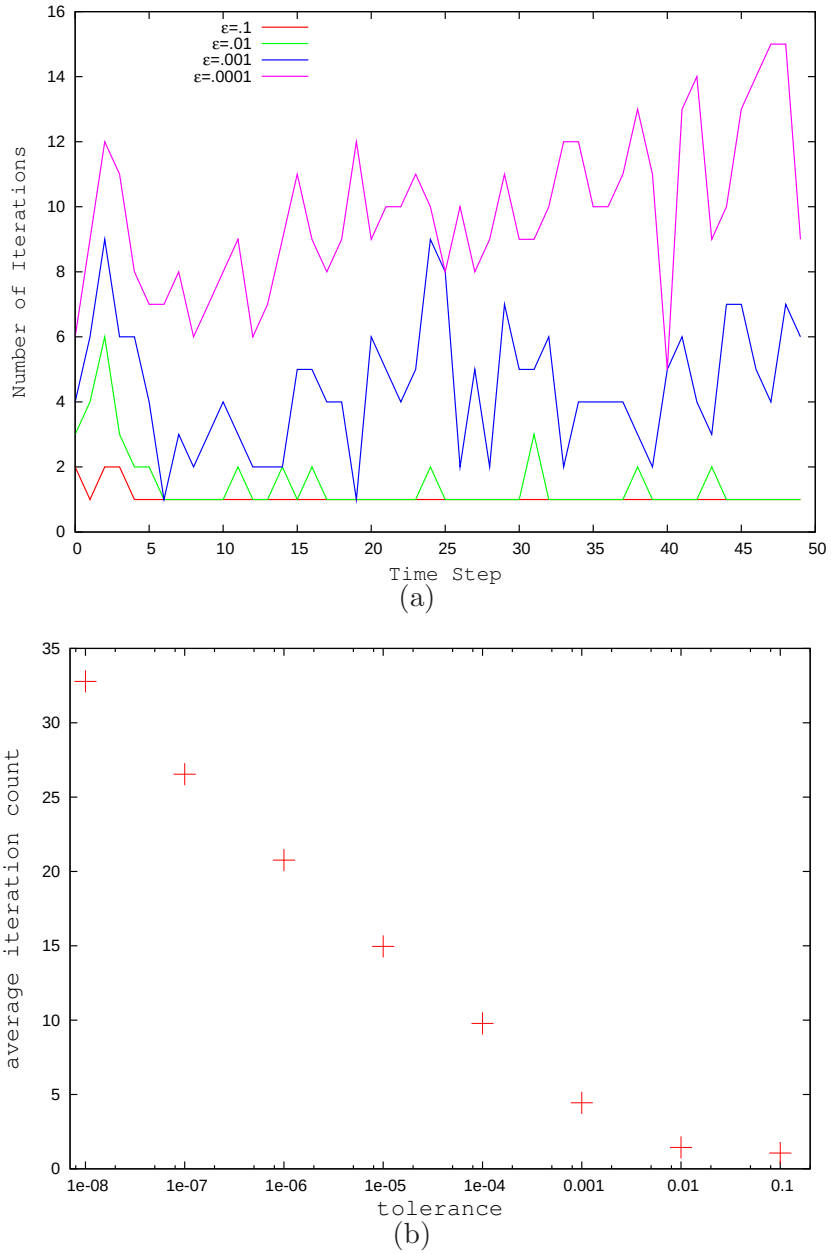

Fig. 2. Panel (a) shows the number of iterations per time step for the first 50 time steps for various values of the tolerance, ε. Panel (b) shows the average number of iterations needed for convergence as a function of tolerance.

gence. For values of $\varepsilon \leq .01$, our solutions are visibly indistinguishable. We have made no attempts to accelerate the iteration process.

3.2 Thin/Thick Interface example

As already alluded to in the introduction, there are instances when the reference field used in the original difference formulation is a poor approximation for the actual radiation field, leading to noise induced crashes. We give a specific example of such a scenario in what follows.

3.2.1 Problem setup

In this example the slab length is .1 cm, has $\rho C_v = .3$ jerk/cm^3, has reflective boundary conditions applied to the left edge, and is open to vacuum on the right edge. There is an optically thin/thick interface at x_b=.025 cm, where to the left the gray opacity is $\sigma = .003$ cm^{-1}, and to the right is $\sigma = 300$ cm^{-1}. With our zoning, this corresponds to $\approx 5\times10^{-6}$ mean free paths per zone in the thin region, and ≈ 0.5 mean free paths per zone in the thick region. Initially the entire slab has temperature .05 keV. There is no initial radiation field, but a constant volumetric heat source in the optically thin region heats the material there at .95 jerks/cm^3-shake. Because of the volumetric heat source, and the poor coupling to the radiation field in the optically thin region, the temperature of the slab in the optically thin region rises at an almost constant rate.

3.2.2 Original difference formulation

For the original difference formulation, the reference field in the thin region corresponds to the material temperature there. Physically, however, the radiation temperature in the thin region is nowhere near the temperature of the material there because the coupling between the material and the radiation is weak; rather the radiation temperature in the thin region is almost equal to the material temperature at the surface of the thick region where emission and absorption are strong.

One expects the statistical fluctuations due to Monte Carlo transport to be large in the optically thin region, because the actual radiation field deviates significantly from a black body at the local material temperature. Figure 3 confirms this expectation. The temperature of the radiation field as measured by its energy density, shown in red, fluctuates wildly, even at early times when the difference between the material temperatures of the thick and thin regions is small. As this difference increases, fluctuations in the material temperature near the surface of the optically thick region, driven by fluctuations in the radiation energy density, become noticeable. For times larger than those shown in Fig. 3, these fluctuations lead to a code crash. Note that in these plots, the floor temperature of the radiation field (as measured by its energy density,

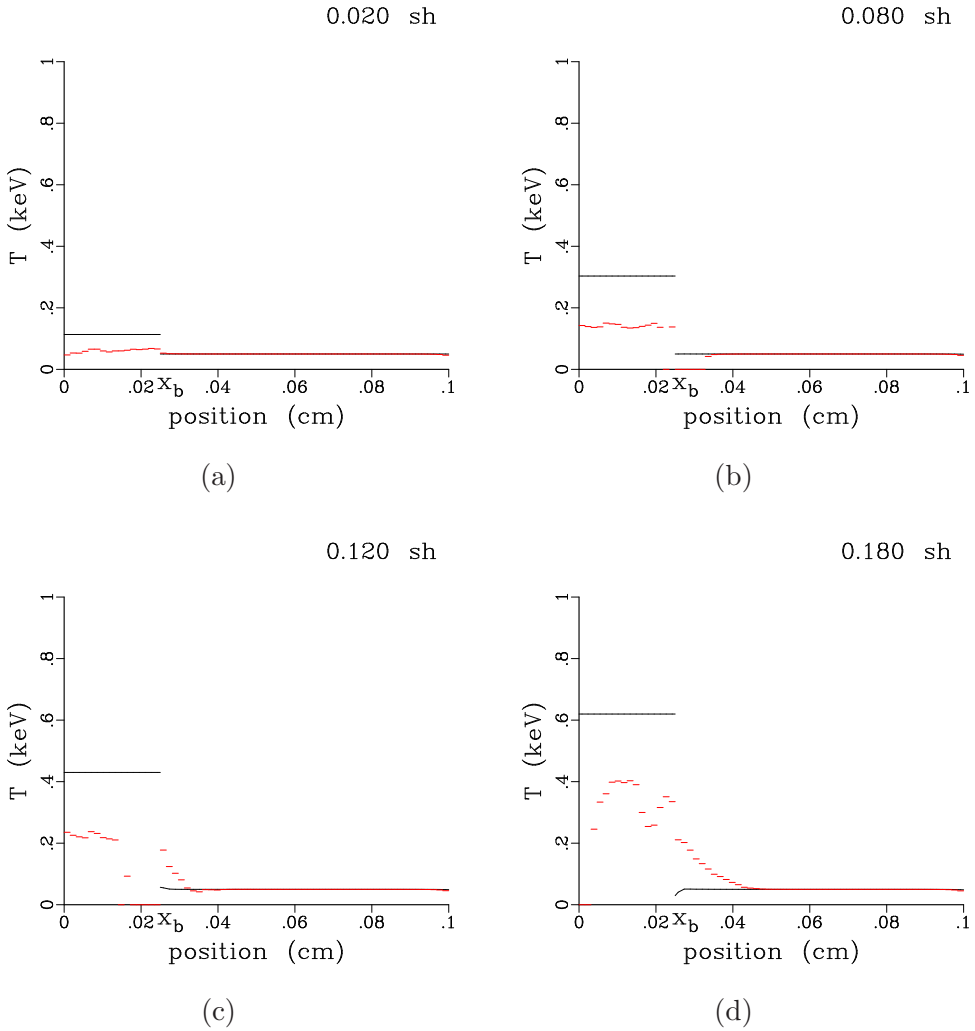

Fig. 3. Results showing radiation temperature as measured by the radiation energy density (red) and material temperature (black) when using the original difference formulation $\overline{B} = B(t)$ at various times. Note the large fluctuations in both radiation and material temperature as the difference in material temperature between the thick and thin regions increases.

aT^4) is set to zero. Negative excursions of the radiation energy density are clipped in the figure, but do occur.

3.2.3 Generalized subtraction scheme

Instead of using a reference field that corresponds to a black body derived from the material temperature in the optically thin region, we now choose $\overline{B}$ in the thin region to be that of the thick region just to the right of x_b, the

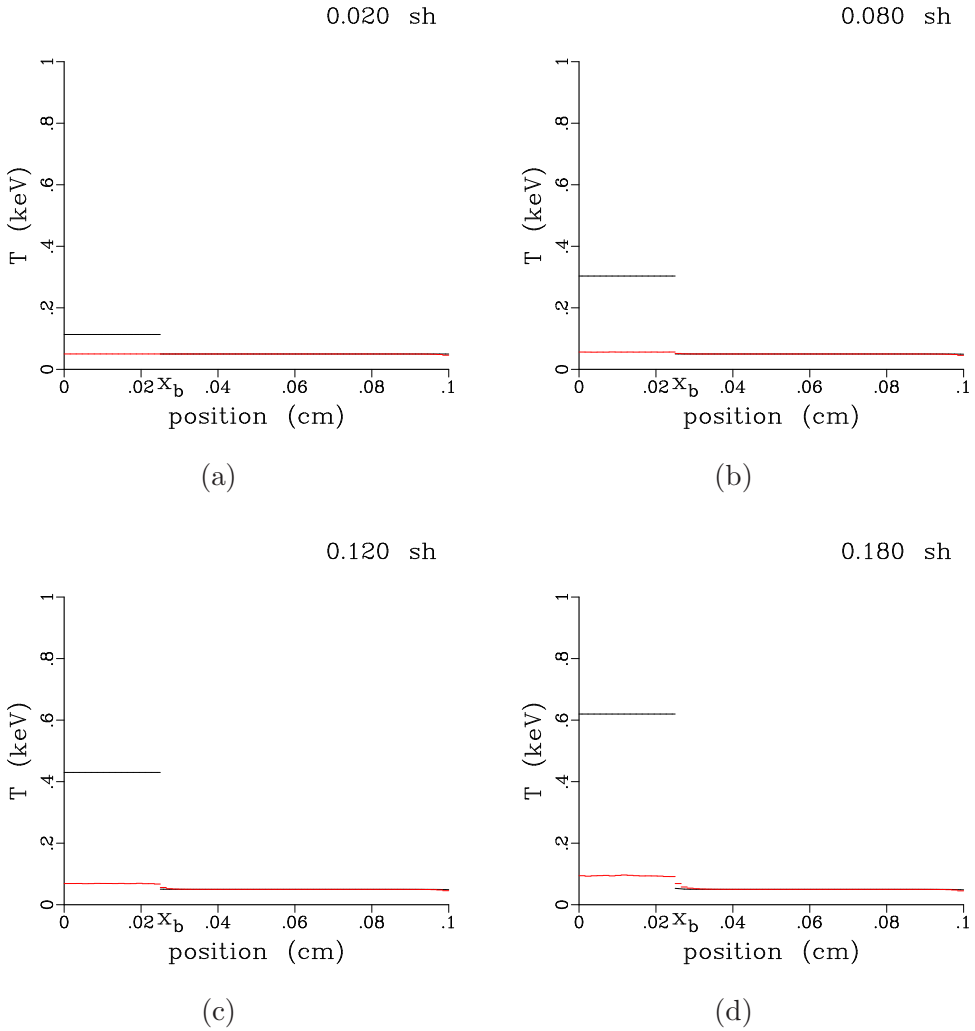

Fig. 4. Results showing radiation temperature (red) and material temperature (black) when using the reference field defined in Eq. (32) at various times. Note the relatively small fluctuations of the radiation temperature as compared to Fig. 3, as well as the stable material temperature profile of the slab.

position of the material interface.

$$\overline{B}(x,t) = \begin{cases} B(x_b, t_0) & \text{if } x < x_b, \;\; t_0 < t \leq (t_0 + \Delta t) \\ B(x, t_0) & \text{if } x \geq x_b, \;\; t_0 < t \leq (t_0 + \Delta t) \end{cases} \tag{32}$$

The arguments of $\overline{B}$ are made explicit to show its dependence on position, as well as time. This particular reference field imposes two slight modifications to the sources shown in Section 2. First, since the reference field is constant in space within the thin region, there are no gradient sources emanating within this region. Second, since the reference field is continuous at the thin/thick interface, there is no delta function source residing at this interface.

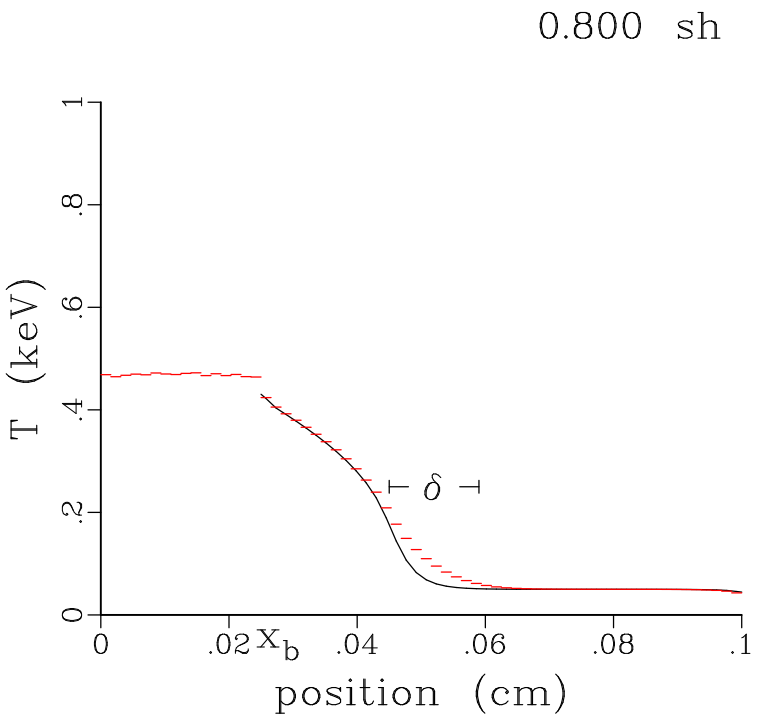

Fig. 5. The same problem as Fig. 4, but after many time steps. Note that due to the constant volumetric source in the thin region, the material temperature in this region is 2.34 keV, well above the range of the figure. Also note the temperature difference between the radiation field and material in the region labeled by δ in the thick region.

As Fig. 4 shows, statistical variations of the radiation temperature as measured by the radiation energy density (red), though still apparent, are much smaller than in Fig. 3. Furthermore, solutions to the material temperature (black) are stable. Indeed, with this choice of reference field, our code does not crash and can run indefinitely. Figure 5 shows the radiation temperature and material temperature after 800 time steps. Because of the constant volumetric heat source in the thin region, the material temperature here is 2.34 keV, well above the 1 keV range of the figure.

As seen from Figs. 4 and 5, the radiation temperature in the thin region is slightly higher than the material temperature of the thick region at the material interface x_b. This difference in radiation temperatures is what drives energy into the thick region. It is clear that the reference field defined in Eq. (32) is a good choice, as the difference field in the thin region is relatively small (but not zero).

Within the thick region the radiation temperature at the leading edge of the Marshak wave is at first larger than the material temperature. As the wave

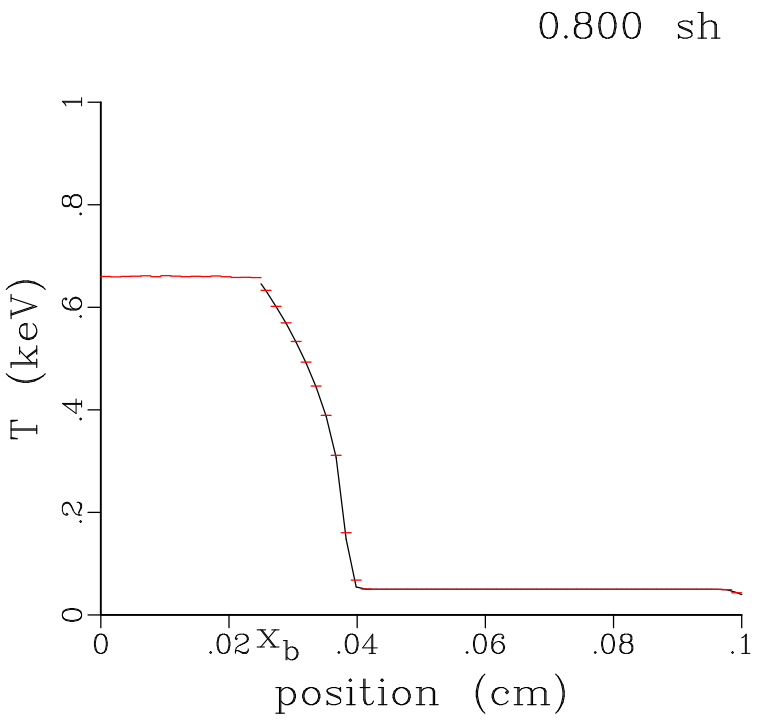

Fig. 6. Similar to Fig. 5, but opacity in the thick region has been increased by an order of magnitude (see text).

propagates, the temperatures relax to each other within a timescale t_{rel} intrinsic to the material, thus the radiation comes into equilibrium (locally) with the material. As derived in Appendix A, t_{rel} is given by

$$t_{rel} = \frac{1}{\beta\sigma c} \quad , \tag{33}$$

where

$$\beta = \frac{4aT^3}{\rho C_v} \quad . \tag{34}$$

For the parameters used in this problem, $t_{rel} \sim .5$ shakes, which is consistent with our results.

Since the material temperature is initially lower than the radiation temperature at the foot of the Marshak wave in the thick region, and thus 'lags' the radiation temperature, there persists a region of width δ where the two temperatures disagree, as shown in Fig. 5. We can estimate how the width of this region, δ, scales with opacity σ. This can be seen by first noting that δ can be approximated by [11]

$$\delta \sim t_{rel} v_{mw} \quad , \tag{35}$$

where v_{mw} represents the velocity of the Marshak wave [12]

$$v_{mw}(t) \sim \frac{1}{2}\sqrt{\frac{\kappa}{\rho C_v t}} \quad . \tag{36}$$

For gray opacities, the coefficient of radiative heat conduction, κ, is given by

$$\kappa \approx \frac{4ca}{3\sigma}T^3 \quad . \tag{37}$$

Combining these expressions gives

$$\delta \sim \frac{1}{\sqrt{12\beta}\ \sqrt{ct}\ \sigma^{3/2}} \quad , \tag{38}$$

which shows that δ scales as $\sigma^{-3/2}$. This suggests that as the medium becomes thicker, the gap decreases (as expected). Figure 6 qualitatively supports this statement, where a calculation analogous to the one presented in Fig. 5 is shown, but the opacity in the thick region is increased by an order of magnitude (σ =3000 cm^{-1}). The gap in this case is too small to be seen in the figure.

4 Stability Analysis

The overwhelming importance of unconditional numerical stability demands that transport calculations in the standard formulation for transport, Eqs. (1) and (2), be done fully implicitly in time. The numerical stability of Monte Carlo calculations is usually difficult to quantify, especially in optically thick, diffusive regions. In such regions there are large emission and absorption terms in the transport equation that nearly cancel, but their noise is additive. The noise masks the signature of the instability, making comparison with a stability analysis difficult. The code suddenly crashes when physical variables enter unphysical territory. Was the problem that caused the crash an instability, or just some other algorithmic fault? It can be hard to tell. The difference formulation solved the noise problem, so it is appropriate to compare our numerical results with theoretical calculations.

We restrict our analysis to optically thick zones and slab geometry. We also assume no energy sources or sinks and we assume that the system is close to equilibrium, in a diffusive regime. We give now qualitative arguments that these conditions are the most unstable ones. Consider an interface between two optically thick zones and assume that there is a small temperature difference between them. (The temperature difference may even be caused by Monte Carlo noise.) We will call the hotter one zone 1 and the colder one zone 2. The difference in temperature causes a flux of radiation to flow from zone 1

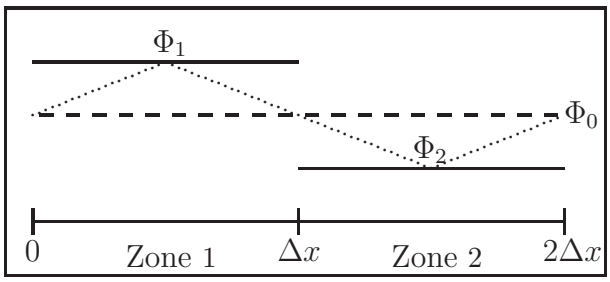

Fig. 7. Initial conditions for performing stability analysis. Periodic boundary conditions are used, photons that exit the problem at $x = 2\Delta x$ re-enter at $x = 0$, and vice versa. The dotted line is the interpolation of Φ between zone centers that is used for the gradient source term, the other source terms use the constant representation of Φ within a zone. The dashed line at Φ_0 is the equilibrium energy density. The deviations from it are small. There is no initial difference field.

to zone 2. When the zones are optically thick, the flow does not depend on the conditions of the other zones. Also, all photons that are emitted in one of the zones – and penetrate into the other zone – are absorbed there. Let us consider what happens in one time step. In reality, the temperature difference diminishes and so does the flux. In our discretization schemes the conditions in each zone are constant during the time step, so radiation flows at a steady rate. If the time step is long enough, and the heat capacity of zones 1 and 2 are small enough, zone 2 can get hotter than zone 1, so the temperature difference becomes oscillatory. The absolute temperature difference may even increase in a time step: this is the cause of numerical instability.

Our experience with the Monte Carlo code implementations discussed in this paper, consistent with the description above, is that short wavelength instabilities dominate. We perform our analysis in the optically thick limit, employing a two zone problem with periodic boundary conditions, expecting that we can capture the behavior we observe. Initial conditions are shown in Fig. 7. The initial difference field is zero. It is useful to write $\Phi_1 = \Phi_0 + \Delta\Phi_1$ and $\Phi_2 = \Phi_0 + \Delta\Phi_2$, as we are interested in small perturbations, $|\Delta\Phi_i| \ll \Phi_0$, with the optically thick limit providing the constraints $1/\sigma\Delta x \ll 1$ and $1/\sigma c\Delta t \ll 1$. These constraints allow for a simplified, but by no means simple, derivation of the sources and their contributions to the energy balance of the (two) zones. The periodic boundary conditions imply that all particles that exit to the right of $x = 2\Delta x$ immediately enter at $x = 0$, and vice versa for particles exiting to the left.

The stability analysis, for each case that we consider, is organized as follows. For each source term appearing in the transport equation, we calculate its energy deposition in the zone in which the particles were born, as well as in the adjacent zone. Because we are in the thick limit, with $e^{-\sigma\Delta x} \approx 0$, radiation does not propagate further than into the zone adjacent to its birth zone and we neglect this possibility. Energy depositions, and holdover energy (the photons

still in flight at the end of the time step), can be calculated to all orders in $1/\sigma\Delta x$ and $1/\sigma c\Delta t$, as we do in Appendix B, but we drop higher order terms when appropriate to simplify the analysis. Given the energy depositions from the source terms, the energy equation can be solved for $\Delta\Phi_i(t_0+\Delta t)$ in terms of $\Delta\Phi_i(t_0)$ and then their ratio can be considered.

Stability is obtained if

$$\left|\frac{\Delta\Phi_i(t_0+\Delta t)}{\Delta\Phi_i(t_0)}\right| < 1 \quad , \tag{39}$$

assuring that the perturbation shrinks with time. The above constraint does not imply monotonic temporal behavior. This occurs only if

$$0 \leq \frac{\Delta\Phi_i(t_0+\Delta t)}{\Delta\Phi_i(t_0)} < 1 \quad . \tag{40}$$

To minimize clutter we introduce the following notation:

$$\varepsilon_x \equiv \frac{1}{\sigma\Delta x} \quad , \tag{41}$$

$$\varepsilon_t \equiv \frac{1}{\sigma\Delta t c} \quad ,$$

$$\gamma \equiv \frac{c\Delta t}{\Delta x} \quad . \tag{42}$$

Thus the assumptions that $1/\sigma\Delta x \ll 1$ and $1/\sigma c\Delta t \ll 1$ are equivalent to $\varepsilon_x \ll 1$ and $\varepsilon_t \ll 1$, respectively.

We now analyze the ratios given by Eq. (39) and Eq. (40) for our differencing schemes. We begin by first formally integrating Eq. (10) from t_0 to $t_0+\Delta t$ and x_i to $x_i+\Delta x$, where x_i is the left edge of zone i. Using the piecewise-constant discretization of the material properties, this gives

$$\Delta x(E_i(t_0+\Delta t) - E_i(t_0)) = 2\pi \int_{x_i}^{x_i+\Delta x} dx \int_{t_0}^{t_0+\Delta t} dt \int d\nu\, d\mu\, \sigma D \\ - 2\pi\Delta t\Delta x \int d\nu\, d\mu\, \sigma(B_i - \overline{B}_i) \quad . \tag{43}$$

Here $E_i = \rho C_v T_i$ is the piecewise-constant value of the material energy and $\sigma(B_i - \overline{B}_i)$ is the piecewise-constant value of the remainder source term in zone i. Since we assume a gray opacity, the right hand side of Eq. (43) can be further simplified by noting that

$$\int d\nu\, d\mu\, (B_i - \overline{B}_i) = \frac{c}{2\pi}(\Phi_i - \overline{\Phi}_i) = \frac{c}{2\pi}(\Delta\Phi_i - \Delta\overline{\Phi}_i) \quad ,$$

where $\Phi = aT^4$, $\Delta\Phi = \Phi - \Phi_0$ and $\Delta\overline{\Phi} = \overline{\Phi} - \Phi_0$, and where $\overline{\Phi}$ is the energy density associated with the reference field, $\overline{B}$.

Since we are considering small deviations from Φ_0, we expand (linearize) the left hand side of Eq. (43) about Φ_0, giving

$$E_i(t_0+\Delta t) - E_i(t_0) \approx \frac{1}{\beta_0}(\Delta\Phi_i(t_0+\Delta t) - \Delta\Phi_i(t_0)) \quad , \tag{44}$$

where $\beta_0 = 4aT_0^3/\rho C_v$, ρ is the material density and C_v is the constant volume specific heat. Combining these expressions into Eq. (43) gives

$$\begin{aligned}\Delta\Phi_i(t_0+\Delta t) - \Delta\Phi_i(t_0) \approx \frac{\beta_0}{\Delta x} 2\pi \int_{x_i}^{x_i+\Delta x} dx \int_{t_0}^{t_0+\Delta t} dt \int d\nu\, d\mu\, \sigma D \\ - \beta_0 \Delta t \sigma c (\Delta\Phi_i(t_0+\Delta t) - \Delta\overline{\Phi}_i(t_0+\Delta t)) \quad .\end{aligned} \tag{45}$$

We now divide both sides of Eq. (45) by $\Delta\Phi_i(t_0)$ to obtain the form of our stability criterion,

$$\begin{aligned}\frac{\Delta\Phi_i(t_0+\Delta t)}{\Delta\Phi_i(t_0)} \approx 1 + \frac{\beta_0}{\Delta x \Delta\Phi_i(t_0)} \left(2\pi \int_{x_i}^{x_i+\Delta x} dx \int_{t_0}^{t_0+\Delta t} dt \int d\nu\, d\mu\, \sigma D \right) \\ - \frac{\beta_0 \Delta t \sigma c}{\Delta\Phi_i(t_0)} (\Delta\Phi_i(t_0+\Delta t) - \Delta\overline{\Phi}_i(t_0+\Delta t)) \quad .\end{aligned} \tag{46}$$

What remains is to show how the integral (within the large parentheses) on the right hand side of Eq. (46) contributes to the energy deposition of zone i, where D is due to the sources that occur during the time step. We must also show that the holdover energy due to these sources that remains at the end of the time step is either small enough to be ignored, or we must explicitly handle it in the stability analysis.

4.1 Original difference formulation using $\overline{B} = B(t_0+\Delta t)$

For the sake of completeness, and in order to show how the various expressions are born out, we first perform our analysis on the original difference formulation as described in [7] and given by Eqs. (6) and (7). Here the reference field $\overline{B}$ is the *end-of-time-step* value of $B = B(t_0+\Delta t)$. In this case, $\Delta\overline{\Phi}_i(t_0+\Delta t) = \Delta\Phi_i(t_0+\Delta t)$ and Eq. (46) becomes

$$\frac{\Delta\Phi_i(t_0+\Delta t)}{\Delta\Phi_i(t_0)} \approx 1 + \frac{\beta_0}{\Delta x \Delta\Phi_i(t_0)} \left(2\pi \int_{x_i}^{x_i+\Delta x} dx \int_{t_0}^{t_0+\Delta t} dt \int d\nu\, d\mu\, \sigma D \right) \quad . \tag{47}$$

The *implicit* sources that contribute to the energy deposition into the material at zone i, as represented under the integral in Eq. (47), are

$$\begin{aligned} \text{time-derivative source} \quad &: \quad -\delta(t-t_0)\frac{1}{4\pi}\left[\Phi_i(t_0+\Delta t)-\Phi_i(t_0)\right] \quad , \\ \text{gradient source} \quad &: \quad -\frac{\mu c}{4\pi\Delta x}\left[\Phi_{i+1}(t_0+\Delta t)-\Phi_i(t_0+\Delta t)\right] \ , \end{aligned} \tag{48}$$

where, since we are dealing with gray opacities, the integral over the frequency ν has already been performed. The gradient source is the source in the dual zone between the center of zone i and the center of zone $i+1$, as shown by the dotted line in Figure 7.

The time-derivative sources are distributed uniformly within each zone i. The gradient that would otherwise exist only on zone boundaries is distributed uniformly between zone centers, as if being produced by the dotted line interpolation shown in Figure 7. Furthermore, all time-derivative particles are born at the beginning of the time step t_0, whereas the gradient sources are born uniformly in time from t_0 to $t_0+\Delta t$.

The calculation of the energy deposition due to these sources, and any holdover energy at the end of the time step, is tedious and is carried out in detail for each source type in Appendix B. For the time derivative source, the energy deposition in the birth zone for a source of strength A is given by Eq. (B.6), while the energy deposition in the adjacent zone is given by Eq. (B.7). Substituting the strength of the time derivative source in zone i,

$$-\frac{1}{4\pi}\left[\Phi_i(t_0+\Delta t)-\Phi_i(t_0)\right] \quad , \tag{49}$$

we obtain for the energy deposition in zone i due to the time derivative sources,

$$\begin{aligned} \Delta x\left(\frac{1}{2}\epsilon_x-1\right)&\left[\Phi_i(t_0+\Delta t)-\Phi_i(t_0)\right] \\ &-\frac{\Delta x\varepsilon_x}{2}\left[\Phi_{i+1}(t_0+\Delta t)-\Phi_{i+1}(t_0)\right] \quad . \end{aligned} \tag{50}$$

Because these sources are emitted at the beginning of the time step there is no holdover energy from the time derivative sources to account for. With an eye to later results, we add and subtract Φ_0, accordingly, so that the energy deposition in zone i from the time derivative source becomes

$$\begin{aligned} \Delta x\left(\frac{1}{2}\epsilon_x-1\right)&\left[\Delta\Phi_i(t_0+\Delta t)-\Delta\Phi_i(t_0)\right] \\ &-\frac{\Delta x\varepsilon_x}{2}\left[\Delta\Phi_{i+1}(t_0+\Delta t)-\Delta\Phi_{i+1}(t_0)\right] \quad . \end{aligned} \tag{51}$$

The energy deposition, in zone 1, for a gradient source with strength $A\mu$ in the region $\Delta x/2 < x < 3\Delta x/2$, and $-A\mu$ elsewhere, is given by Eq. (B.24), while the total holdover due to this source in zone 1 is given by Eq. (B.25).

Substituting the strength, A, for this source

$$-\frac{c}{4\pi\Delta x}\left[\Phi_2(t_0+\Delta t)-\Phi_1(t_0+\Delta t)\right] \quad , \tag{52}$$

and considering the fact that the absorbed energy for zone 2 is that of zone 1 with the sign reversed, the energy absorbed in zone i is

$$-\frac{2c}{3}\Delta t\varepsilon_x(2\varepsilon_t-1)\left[\Phi_{i+1}(t_0+\Delta t)-\Phi_i(t_0+\Delta t)\right] \quad . \tag{53}$$

Again, adding and subtracting Φ_0, we obtain for the absorbed energy

$$-\frac{2c}{3}\Delta t\varepsilon_x(2\varepsilon_t-1)\left[\Delta\Phi_{i+1}(t_0+\Delta t)-\Delta\Phi_i(t_0+\Delta t)\right] \quad . \tag{54}$$

Similarly, the holdover energy in zone i is

$$\frac{2c}{3}\left[\Delta\Phi_{i+1}(t_0+\Delta t)-\Delta\Phi_i(t_0+\Delta t)\right]\Delta t\varepsilon_t\varepsilon_x \quad . \tag{55}$$

Unlike the time derivative source that has no holdover, the gradient source has a holdover containing a factor $\varepsilon_t\varepsilon_x$. This factor is second order small, and we could complete the stability analysis by ignoring these second order terms, but the presence of the ε_x factor indicates that it came from a position just upstream of a zone interface, and all holdovers come from sources generated near the end of the time step. The holdover will be absorbed at the beginning of the next time step, and it will be absorbed in the zone where it resides as it has just entered it. With that understanding, we now have the energy deposited by the holdover from the *prior time step*,

$$\frac{2c}{3}\left[\Delta\Phi_{i+1}(t_0)-\Delta\Phi_i(t_0)\right]\Delta t\varepsilon_t\varepsilon_x \quad . \tag{56}$$

Because we have linearized, via Eq. (44), the sum of the holdovers in each zone, Eq. (56), is zero, and our algorithm is energy conserving, any shift in zone i must be accompanied by an equal, but opposite shift in zone $i+1$. That is,

$$\Delta\Phi_{i+1}=-\Delta\Phi_i \quad . \tag{57}$$

The energy deposited by the D field during the time step is the sum of Eqs. (51), (54) and (56). Using Eq. (57), the sum of the energy depositions in zone i is

$$\begin{aligned}\left(\Delta x(\varepsilon_x-1)+\frac{4c}{3}\Delta t\varepsilon_x(2\varepsilon_t-1)\right)\Delta\Phi_i(t_0+\Delta t)\\ +\left[\Delta x(1-\varepsilon_x)-\frac{4c}{3}\Delta t\varepsilon_t\varepsilon_x\right]\Delta\Phi_i(t_0) \quad .\end{aligned} \tag{58}$$

Substituting the sum for the energy deposition in zone i, Eq. (58), into Eq. (47) (replacing the integral in the large parentheses including the factor of 2π), and performing some algebra, gives

$$\frac{\Delta\Phi_i(t_0+\Delta t)}{\Delta\Phi_i(t_0)} \approx \frac{1+\beta_0\left[1-\varepsilon_x-\frac{4}{3}\gamma\varepsilon_t\varepsilon_x\right]}{1+\beta_0\left(1-\varepsilon_x+\frac{4}{3}\gamma\varepsilon_x(1-2\varepsilon_t)\right)} \quad . \tag{59}$$

The role of the $\approx$ sign is to remind us that we have linearized the treatment of the material energy via Eq. (44), and that we have dropped terms with factors $e^{-\sigma\Delta x}$, or $e^{-\sigma c\Delta t}$, in the computation of energy depositions in Appendix B, but we have otherwise carried all orders of ε_t and ε_x. Given that β_0 is positive and that ε_t and ε_x are small positive quantities, the ratio is positive and less than one. The method is therefore unconditionally stable and monotonic in time.

4.2 Generalized subtraction using $\overline{B} = B(t_o)$

Because of the subtraction of the value of B *at the beginning of the time step*, Eq. (46) becomes

$$\frac{\Delta\Phi_i(t_0+\Delta t)}{\Delta\Phi_i(t_0)} \approx 1+\frac{\beta_0}{\Delta x\Delta\Phi_i(t_0)}\left(2\pi\int_{x_i}^{x_i+\Delta x}dx\int_{t_0}^{t_0+\Delta t}dt\int d\nu d\mu\sigma D\right) - \frac{\beta_0\Delta t\sigma c}{\Delta\Phi_i(t_0)}(\Delta\Phi_i(t_0+\Delta t)-\Delta\Phi_i(t_0)) \quad . \tag{60}$$

The sources are now

$$\begin{aligned} \text{time-derivative source} \quad &: \quad -\delta(t-t_0)\frac{1}{4\pi}\left[\Phi_i(t_0)-\Phi_i(t_0-\Delta t)\right] \quad , \\ \text{gradient source} \quad &: \quad -\frac{\mu c}{4\pi\Delta x}\left[\Phi_{i+1}(t_0)-\Phi_i(t_0)\right] \quad , \\ \text{remainder source} \quad &: \quad \frac{c\sigma}{4\pi}\left[\Phi_i(t_0+\Delta t)-\Phi_i(t_0)\right] \quad . \end{aligned} \tag{61}$$

where we have again integrated over frequency as we are dealing with gray opacities. Only the remainder source depends upon the unknown $\Phi(t_0+\Delta t)$.

Comparing Eq. (61) to Eq. (48), the time derivative and gradient sources are obtained by making the replacement $t_0 \rightarrow t_0-\Delta t$. The energy deposition from the time derivative source is obtained by making this same replacement in Eq. (51),

$$\Delta x\left(\frac{1}{2}\epsilon_x-1\right)\left[\Delta\Phi_i(t_0)-\Delta\Phi_i(t_0-\Delta t)\right] - \frac{\Delta x\varepsilon_x}{2}\left[\Delta\Phi_{i+1}(t_0)-\Delta\Phi_{i+1}(t_0-\Delta t)\right] \quad . \tag{62}$$

The energy deposition from the gradient source is obtained by making this replacement in Eq. (54),

$$-\frac{2c}{3}\Delta t\varepsilon_x(2\varepsilon_t-1)\left[\Delta\Phi_{i+1}(t_0)-\Delta\Phi_i(t_0)\right] \quad . \tag{63}$$

The holdover energy in zone i, from the gradient source in the *prior time step*, is obtained by making this replacement in Eq. (56),

$$\frac{2c}{3}\left[\Delta\Phi_{i+1}(t_0-\Delta t)-\Delta\Phi_i(t_0-\Delta t)\right]\Delta t\varepsilon_t\varepsilon_x \quad . \tag{64}$$

We are left with the remainder source of Eq. (61). This source is isotropic and uniform in both space and time. The energy deposited in the birth zone is given by Eq.(B.14), using

$$\frac{c\sigma}{4\pi}\left[\Delta\Phi_i(t_0+\Delta t)-\Delta\Phi_i(t_0)\right] \tag{65}$$

for the source strength, A. We have added and subtracted Φ_0 in order to get the source strength in terms of $\Delta\Phi_i$. The energy deposited in zone i due to the remainder source from zone i, then, is

$$\frac{c\sigma}{2}\left[\Delta\Phi_i(t_0+\Delta t)-\Delta\Phi_i(t_0)\right]\Delta t\Delta x\left(2-2\varepsilon_t-\varepsilon_x+2\varepsilon_t\varepsilon_x\right) \quad . \tag{66}$$

Similarly, using Eq. (B.13), the holdover energy in zone i due to the remainder source from zone i, from the prior time step, is

$$\frac{c\sigma}{2}\left[\Delta\Phi_i(t_0)-\Delta\Phi_i(t_0-\Delta t)\right]\Delta t\Delta x\varepsilon_t\left(2-\varepsilon_x\right) \quad . \tag{67}$$

The energy deposited in zone i due to the remainder source born in zone $i+1$ is given by Eq. (B.12), substituting A,

$$\frac{c\sigma}{2}\left[\Delta\Phi_{i+1}(t_0+\Delta t)-\Delta\Phi_{i+1}(t_0)\right]\Delta t\Delta x\varepsilon_x\left(1-2\varepsilon_t\right) \quad . \tag{68}$$

The holdover in zone i due to the remainder source born in zone $i+1$ is given by Eq. (B.11), substituting A for the prior time step,

$$\frac{c\sigma}{2}\left[\Delta\Phi_{i+1}(t_0)-\Delta\Phi_{i+1}(t_0-\Delta t)\right]\Delta t\Delta x\varepsilon_t\varepsilon_x \quad . \tag{69}$$

The assertion that $\Delta\Phi_{i+1}=-\Delta\Phi_i$ does not come as easily as it did for Section 4.1, but the argument that the dynamics preserves this relationship goes as follows. We have an initial condition that $\Delta\Phi_{i+1}(0)=-\Delta\Phi_i(0)$. There is no time derivative source for the first time step. The energy deposition from the gradient source will drive the zone with the positive $\Delta\Phi$ down, and the zone with the negative $\Delta\Phi$ up, by the same amount. These changes produce

equal, and opposite, remainder sources in each zone, with equal and opposite holdovers. At the end of the time step, therefore, the self consistent solution will be $\Delta\Phi_{i+1}(\Delta t) = -\Delta\Phi_i(\Delta t)$, with the holdover having opposite sign for each zone. For the second time step, we have a time derivative source that derives from the equal and opposite change in $\Delta\Phi$ that transpired in the first time step. When this, and the holdover from the prior time step, is thrown in to the dynamic that we have already described for the first time step, the relationship, $\Delta\Phi_{i+1} = -\Delta\Phi_i$, is still preserved, and by induction, for all time steps.

The energy absorbed in zone i, dropping terms proportional to $\varepsilon_t\varepsilon_x$ so that we need not worry with holdover in zone i that escapes to zone $i+1$ before it is absorbed, is the sum of Eqs. (62), (63), (66), (67) and (68). The sum of these terms, using $\Delta\Phi_{i+1} = -\Delta\Phi_i$ and dropping terms proportional to $\varepsilon_t\varepsilon_x$, is

$$\begin{aligned}
&\Delta x\,(\epsilon_x - 1)\,[\Delta\Phi_i(t_0) - \Delta\Phi_i(t_0 - \Delta t)] \\
&\qquad - \frac{4c}{3}\Delta t\varepsilon_x\Delta\Phi_i(t_0) \\
&\quad + \frac{c\sigma}{2}\,[\Delta\Phi_i(t_0 + \Delta t) - \Delta\Phi_i(t_0)]\,\Delta t\Delta x\,(2 - 2\varepsilon_t - \varepsilon_x) \\
&\qquad + c\sigma\,[\Delta\Phi_i(t_0) - \Delta\Phi_i(t_0 - \Delta t)]\,\Delta t\Delta x\varepsilon_t \\
&\qquad - \frac{c\sigma}{2}\,[\Delta\Phi_i(t_0 + \Delta t) - \Delta\Phi_i(t_0)]\,\Delta t\Delta x\varepsilon_x \quad . \quad (70)
\end{aligned}$$

With an eye for what is to come, we factor out $\Delta\Phi_i(t_0 + \Delta t)$, $\Delta\Phi_i(t_0)$, and $\Delta\Phi_i(t_0 - \Delta t)$, obtaining the energy deposition in zone i, the integral in parentheses in Eq.(60), in a form useful for what will follow below,

$$\begin{aligned}
&(-\Delta x + c\Delta t(\sigma\Delta x - 1))\,\Delta\Phi_i(t_0 + \Delta t) \\
&\qquad + \left(\Delta x(1 + \varepsilon_x) + c\Delta t(1 - \frac{4\varepsilon_x}{3} - \sigma\Delta x)\right)\Delta\Phi_i(t_0) \\
&\qquad - \Delta x\varepsilon_x\Delta\Phi_i(t_0 - \Delta t) \quad . \quad (71)
\end{aligned}$$

Substituting, and using $c\Delta t/\Delta x = \gamma$, we obtain for Eq. (60),

$$\begin{aligned}
&(1 + \beta_0(1 + \gamma))\frac{\Delta\Phi_i(t_0 + \Delta t)}{\Delta\Phi_i(t_0)} \\
&\qquad - 1 - \beta_0\left(1 + \varepsilon_x + \gamma(1 - \frac{4\varepsilon_x}{3})\right) \\
&\qquad + \beta_0\varepsilon_x\frac{\Delta\Phi_i(t_0 - \Delta t)}{\Delta\Phi_i(t_0)} \approx 0 \quad . \quad (72)
\end{aligned}$$

Unlike in the previous section where the ratio $\Delta\Phi(t_0 + \Delta t)/\Delta\Phi(t_0)$ could be solved for directly, the dependence on $\Delta\Phi_i(t_0 - \Delta t)$ requires us to solve a

recurrence relation. A detailed solution, given the initial conditions, can be solved for, but our interest is only in learning whether the solution is growing or shrinking, asymptotically. To this end, we make the substitutions

$$\begin{aligned}\frac{\Delta\Phi_i(t_0+\Delta t)}{\Delta\Phi_i(t_0)} &= \alpha \quad , \\ \frac{\Delta\Phi_i(t_0-\Delta t)}{\Delta\Phi_i(t_0)} &= \frac{1}{\alpha} \quad ,\end{aligned}$$

in Eq. (72), obtaining,

$$(1+\beta_0(1+\gamma))\alpha - 1 - \beta_0\left(1+\varepsilon_x+\gamma(1-\frac{4\varepsilon_x}{3})\right) + \beta_0\varepsilon_x\frac{1}{\alpha} \approx 0 \quad . \qquad (73)$$

The solution for α requires solving a quadratic equation. Thus there are two solutions. To facilitate the presentation, we expand the two solutions to order ε_x,

$$\alpha = \begin{cases} 1 - \varepsilon_x\frac{4}{3}\frac{\beta_0\gamma}{1+\beta_0(2+\gamma)} + O(\varepsilon_x^2, \varepsilon_x\varepsilon_t) \quad , \\ \varepsilon_x\frac{\beta_0}{1+\beta_0(1+\gamma)} + O(\varepsilon_x^2, \varepsilon_x\varepsilon_t) \quad . \end{cases} \qquad (74)$$

The solutions above represent the two allowed 'modes' of the recurrence relation, which characterize the long-time behavior of this system. A general solution to the recurrence equations will involve a linear combination of both modes. α is positive and less than 1 for both modes, indicating that the general solution is stable and monotonic in time.

4.3 Talyor expansion of $\sigma(B-\overline{B})$

We now consider the case of fully explicit sources, wherein we approximate the implicit remainder source by its *explicit* first order Taylor expansion,

$$\begin{aligned}\sigma\left(B(t)-\overline{B}(t)\right) &= \sigma\left(B(t)-B(t-\Delta t)\right) \\ &\approx \sigma\Delta t\frac{\partial B(t)}{\partial t} \qquad (\Delta t \ll t_{rel}) \quad . \qquad (75)\end{aligned}$$

The lack of any implicit sources makes this discretization method susceptible to instability, which is born out in our stability analysis below.

The sources in this case become

$$\begin{aligned}
\text{time derivative source} &: -\delta(t-t_0)\frac{1}{4\pi}\left[\Phi_i(t_0)-\Phi_i(t_0-\Delta t)\right] \quad , \\
\text{gradient source} &: -\frac{\mu c}{4\pi\Delta x}\left[\Phi_{i+1}(t_0)-\Phi_i(t_0)\right] \quad , \\
\text{explicit remainder source} &: \frac{c\sigma}{4\pi}\left[\Phi_i(t_0)-\Phi_i(t_0-\Delta t)\right] \quad . \qquad (76)
\end{aligned}$$

It is easy to see that Eq. (46) becomes

$$\begin{aligned}
\frac{\Delta\Phi_i(t_0+\Delta t)}{\Delta\Phi_i(t_0)} \approx 1 + \frac{\beta_0}{\Delta x \Delta\Phi_i(t_0)}\left(2\pi\int_{x_i}^{x_i+\Delta x}dx\int_{t_0}^{t_0+\Delta t}dt\int d\nu d\mu\sigma D\right) \\
-\frac{\beta_0\Delta t\sigma c}{\Delta\Phi_i(t_0)}(\Delta\Phi_i(t_0)-\Delta\Phi_i(t_0-\Delta t)) \quad . \quad (77)
\end{aligned}$$

Comparing Eq. (76) to Eq. (61), we see that the energy deposition is obtained by making the substitution $(\Phi_i(t_0+\Delta t)-\Phi_i(t_0)) \rightarrow (\Phi_i(t_0)-\Phi_i(t_0-\Delta t))$ in the terms arising from the remainder source (those with an explicit factor of σ) in Eq. (70),

$$\begin{aligned}
&\Delta x\,(\epsilon_x-1)\left[\Delta\Phi_i(t_0)-\Delta\Phi_i(t_0-\Delta t)\right] \\
&\qquad -\frac{4c}{3}\Delta t\varepsilon_x\Delta\Phi_i(t_0) \\
&\quad +\frac{c\sigma}{2}\left[\Delta\Phi_i(t_0)-\Delta\Phi_i(t_0-\Delta t)\right]\Delta t\Delta x\,(2-2\varepsilon_t-\varepsilon_x) \\
&\qquad +c\sigma\left[\Delta\Phi_i(t_0-\Delta t)-\Delta\Phi_i(t_0-2\Delta t)\right]\Delta t\Delta x\varepsilon_t \\
&\qquad -\frac{c\sigma}{2}\left[\Delta\Phi_i(t_0)-\Delta\Phi_i(t_0-\Delta t)\right]\Delta t\Delta x\varepsilon_x \quad . \quad (78)
\end{aligned}$$

Substitution of this energy deposition into Eq. (77) leads to a cubic equation that we must find the roots of in order to obtain the growth coefficients. To make understanding the results less problematic, we consider the case that $\varepsilon_t << \varepsilon_x$, or equivalently, large γ. Dropping the terms proportional to ε_t, we obtain

$$\begin{aligned}
&\Delta x\,(\epsilon_x-1)\left[\Delta\Phi_i(t_0)-\Delta\Phi_i(t_0-\Delta t)\right] \\
&\qquad -\frac{4c}{3}\Delta t\varepsilon_x\Delta\Phi_i(t_0) \\
&\quad +\frac{c\sigma}{2}\left[\Delta\Phi_i(t_0)-\Delta\Phi_i(t_0-\Delta t)\right]\Delta t\Delta x\,(2-\varepsilon_x) \\
&\qquad -\frac{c\sigma}{2}\left[\Delta\Phi_i(t_0)-\Delta\Phi_i(t_0-\Delta t)\right]\Delta t\Delta x\varepsilon_x \quad . \quad (79)
\end{aligned}$$

Collecting coefficients of $\Delta\Phi_i(t_0)$ and $\Delta\Phi_i(t_0-\Delta t)$ gives,

$$\begin{aligned}
&\left(\Delta x(\varepsilon_x-1)-c\Delta t(1+\frac{4}{3}\varepsilon_x-\sigma\Delta x)\right)\Delta\Phi_i(t_0) \\
&\qquad (\Delta x(1-\varepsilon_x)+c\Delta t(1-\sigma\Delta x))\Delta\Phi_i(t_0-\Delta t) \quad . \quad (80)
\end{aligned}$$

Substituting this for the energy deposition term in Eq. (77) (the integral in the parentheses) we obtain,

$$\frac{\Delta\Phi_i(t_0+\Delta t)}{\Delta\Phi_i(t_0)} + \beta_0\left(1+\gamma+\varepsilon_x\left(\frac{4}{3}\gamma-1\right)\right) - 1 \\ + \beta_0(\varepsilon_x-\gamma-1)\frac{\Delta\Phi_i(t_0-\Delta t)}{\Delta\Phi_i(t_0)} \approx 0 \quad . \quad (81)$$

As in the prior section, we make the substitutions

$$\frac{\Delta\Phi_i(t_0+\Delta t)}{\Delta\Phi_i(t_0)} = \alpha \quad , \\ \frac{\Delta\Phi_i(t_0-\Delta t)}{\Delta\Phi_i(t_0)} = \frac{1}{\alpha} \quad ,$$

in Eq. (81), obtaining,

$$\alpha + \beta_0\left(1+\gamma+\varepsilon_x\left(\frac{4}{3}\gamma-1\right)\right) - 1 + \beta_0(\varepsilon_x-\gamma-1)\frac{1}{\alpha} \approx 0 \quad . \quad (82)$$

We expand the solutions for α to first order in ϵ_x, obtaining

$$\alpha = \begin{cases} 1-\varepsilon_x\frac{4}{3}\frac{\beta_0\gamma}{1+\beta_0(1+\gamma)} + O(\varepsilon_x^2, \varepsilon_x\varepsilon_t) \quad , \\ -\beta_0(1+\gamma) + \varepsilon_x\frac{\beta_0(6-2\beta_0(\gamma(1+4\gamma)-3)}{6(1+\beta_0(1+\gamma))} + O(\varepsilon_x^2, \varepsilon_x\varepsilon_t) \quad . \end{cases} \quad (83)$$

One of the modes will be unstable when

$$\beta_0\,(1+\gamma) > 1 \quad ,$$

or, equivalently, when

$$\gamma = \frac{c\Delta t}{\Delta x} > \left(\frac{1}{\beta_0}-1\right) \quad . \quad (84)$$

In Figure 8, we plot $\Delta t = \Delta x(\beta_0^{-1}-1)/c$ (the black line) for the particular parameters labeled in the figure. Runs with randomly sampled initial temperatures, T_0, and time step sizes, Δt, were performed with initial conditions shown in Fig. 7. Stability was determined by examining the growth, or shrinkage, of an initial perturbation in Φ for a two zone problem with periodic boundary conditions. Runs that were stable are plotted in green, whereas unstable runs are shown in red. Note that the demarcation between stable and unstable is well predicted by the black line.

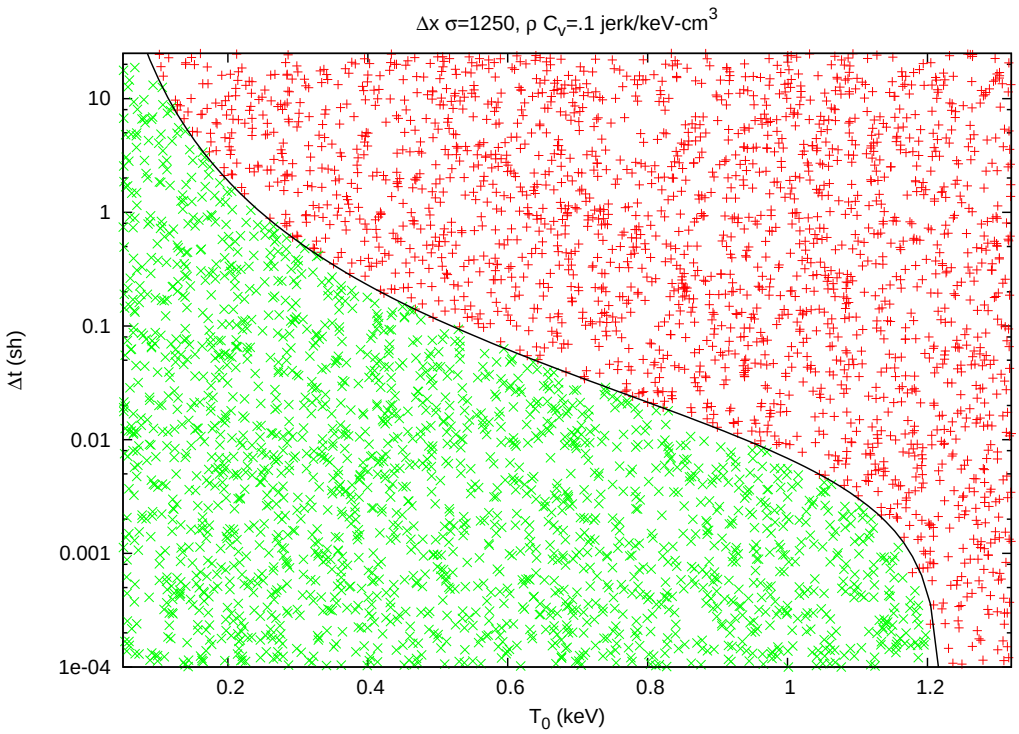

Fig. 8. Scatter plot showing numerical results that demarcate stable, green, and unstable, red, runs. The solid black line is the derived stability criterion given by Eq. (84). The zone size, Δx, is 2.5cm.

5 Conclusion

In this report, we have evaluated generalizations of the difference formulation that use reference fields other than the black body corresponding to the implicitly differenced local material temperature. We have shown that by using the black body corresponding to the material temperature at the beginning of the time step, the remainder of the thermal emission term is small when the problem is slowly varying. This provides a material energy equation that is amenable to a fast iterative solution and addresses the cost associated with the Newton-Raphson solve that is required in the original difference formulation.

In problems with optically thin regions adjacent to optically thick ones, cancellation of the gradient source terms can cause high levels of noise in Monte Carlo solutions, with attendant problem crashes. To resolve this problem we have explored using the black body corresponding to the adjacent optically thick region for the reference field in the optically thin region, finding that it removes the noise induced problem crashes.

In addition to numerical results, we have explored the stability of our discretizations of the difference formulation in the optically thick limit. We find our generalized difference formulation to be unconditionally stable.

A Derivation of relaxation time t_{rel} of material

Here we make the assumption that the radiation field is held constant, while the material temperature, T_{mat}, is allowed to change. The change in material energy is given by

$$\frac{\partial E_{mat}}{\partial t} = \frac{1}{\beta}\frac{\partial \Phi_{mat}}{\partial t} = \int d\nu \, d\Omega \; (I - B_{mat}(t)) \quad , \tag{A.1}$$

where

$$\beta = \frac{4a^{1/4}}{\rho C_v} T_{mat}^3 \quad .$$

For grey opacities, the right hand side of Eq. (A.1) can be expressed as

$$\int d\nu \, d\Omega \; (I - B_{mat}(t)) = c\sigma \left[\Phi_{rad} - \Phi_{mat}(t)\right] \quad ,$$

where we have identified the constant radiation density with $\Phi_{rad} = a\, T_{rad}^4$. Let us further assume that T_{rad} is not too different from T_{mat}.

The solution to Eq. (A.1) is simply

$$\Phi_{mat}(t) = \Phi_{rad} - C\, e^{-\beta\sigma\, c\, t} \quad ,$$

where C is some constant that depends on the initial conditions. The argument of the exponential defines the relaxation time of the material, giving us the desired result

$$t_{rel} = \frac{1}{\beta\sigma c} \quad .$$

B Energy Depositions

Here we derive the absorbed energy and the holdover energy remaining at the end of the time step (photons still in flight) for the source types required by the stability analysis of Section 4. We consider sources of strength A, or μA, distributed in time and space as required for the discretizations that we consider. These results are used as generic expressions, substituting the actual source strength, to compute the energy deposition and holdover energy for the situations covered in the stability analysis.

The energy depositions are for a two zone problem with periodic boundary conditions where each zone is of width Δx, having an opacity σ, with the source of the D field emitted and propagated for the duration of the time step, Δt. We are interested in the thick limit where $\sigma\Delta x >> 1$ and $\sigma c\Delta t >> 1$; and,

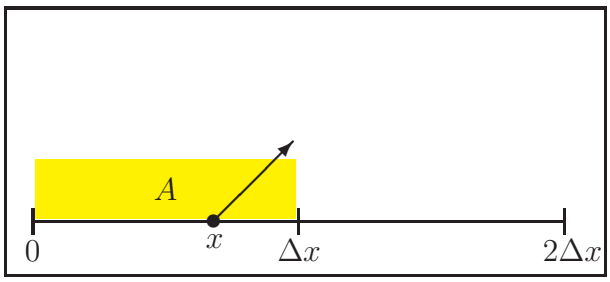

Fig. B.1. A depiction of a uniform isotropic source of strength A in one zone. The region shaded yellow is marking the zone with the source. The x axis is the position through the slab, while the unlabeled y axis is the position along the slab. A Monte Carlo particle born at position x, traveling in the direction shown by the arrow, travels a distance $s = (\Delta x - x)/\mu$ before escaping into the adjacent zone, where μ is the cosine of the particle direction with respect to perpendicular direction through the slab. Periodic boundary conditions are used. A Monte Carlo particle exiting the problem at $x = 2\Delta x$ enters again at $x = 0$, and vice versa.

equivalently, $\varepsilon_x \equiv 1/\sigma\Delta x << 1$ and $\varepsilon_t \equiv 1/\sigma\Delta tc << 1$. We ignore terms containing $e^{-\sigma\Delta x}$, or $e^{-\sigma c\Delta t}$, as exponential factors as these are smaller than any power of ε_x or ε_t.

We want, for each source term, the absorbed energy and the holdover energy in each zone. The general strategy that we will use is to compute the total energy emitted by the source in a zone, the total holdover from this emitted energy in both zones, the amount of emitted energy that passes through the zone boundary into the adjacent zone, and then finally its holdover. From these, we can then obtain the energy absorbed and the holdover in each zone by subtraction.

Formally, we want the energy deposition from Eq (43),

$$2\pi \int_{x_{i-1}}^{x_i} dx \int_{t_0}^{t_0+\Delta t} dt \int d\nu \, d\mu \, \sigma D \quad . \tag{B.1}$$

It is easy to show that for a D field represented by Monte Carlo particles of energy weight $w_0 e^{-\sigma s}$, where s is the path length traveled, the energy deposition is 2π times the energy weight lost by the particle. It is from this perspective that we will calculate the energy deposition and holdover energy.

B.1 Uniform, in space, isotropic source of strength A emitted at the beginning of the time step.

To compute the energy deposition and holdover energy in each zone for an isotropic source of strength A emitted at the beginning of the time step, we consider the right moving, $\mu \geq 0$, component of this source as depicted in

Fig. B.1. Using periodic boundary conditions, the additional influence of the left moving component of the source is obtained by multiplying by a factor of 2. The total emitted energy is

$$4\pi \int_0^1 d\mu \int_0^{\Delta x} dx A = 4\pi A \Delta x \quad . \tag{B.2}$$

The holdover energy, without regard for the zone it is in, is

$$4\pi \int_0^1 d\mu \int_0^{\Delta x} dx A e^{-\sigma c \Delta t} = 4\pi A \Delta x e^{-\sigma c \Delta t} \approx 0 \quad , \tag{B.3}$$

and as it contains a factor of $e^{-\sigma c \Delta t}$ it is taken to be zero for the purposes of this analysis. In what follows below in this appendix, we will use the $\approx$ sign to indicate that we have dropped terms including such a factor, but we otherwise carry all orders in ε_x and ε_t. We show this explicitly in some of the earlier integrals that are evaluated, but in the more complicated cases terms with factors of this sort are evaluated and dropped during intermediate integration steps.

As the path length to reach the adjacent zone is $(\Delta x - x)/\mu$, photons born at $x < \Delta x - c\mu\Delta t$ do not have time to reach the next zone. The energy that escapes into the adjacent zone is

$$4\pi \int_0^1 d\mu \int_{\Delta x - c\mu\Delta t}^{\Delta x} dx A e^{-\sigma(\Delta x - x)/\mu} = \frac{2\pi A}{\sigma}(1 - e^{-\sigma c \Delta t}) \approx 2\pi A \Delta x \varepsilon_x \quad . \tag{B.4}$$

The holdover in the adjacent zone is

$$4\pi \int_0^1 d\mu \int_{\Delta x - c\mu\Delta t}^{\Delta x} dx A e^{-\sigma c \Delta t} = 2\pi A c \Delta t e^{-\sigma c \Delta t} \approx 0 \quad . \tag{B.5}$$

As there is no holdover, the energy absorbed in the birth zone is obtained by subtracting the escaped energy, Eq. (B.4), from the emitted energy, Eq. (B.2),

$$2\pi A \Delta x (2 - \varepsilon_x) \quad . \tag{B.6}$$

The energy absorbed in the adjacent zone is simply the energy that escaped into it,

$$2\pi A \Delta x \varepsilon_x \quad . \tag{B.7}$$

B.2 Uniform, in both space and time, isotropic source of strength A.

To compute the energy deposition and holdover energy in each zone for an isotropic source of strength A emitted uniformly during the time step, we again consider the right moving, $\mu \geq 0$ component of this source as depicted in

Fig. B.1. Using periodic boundary conditions, the influence of the left moving component of the source is again obtained by multiplying by a factor of 2. The emitted energy is

$$4\pi \int_0^1 d\mu \int_0^{\Delta t} dt \int_0^{\Delta x} dx A = 4\pi A \Delta t \Delta x \quad . \tag{B.8}$$

The holdover energy, without regard for which zone it is in, is

$$4\pi \int_0^1 d\mu \int_0^{\Delta t} dt \int_0^{\Delta x} dx A e^{-\sigma c(\Delta t - t)} \approx 4\pi A \Delta t \Delta x \varepsilon_t \quad . \tag{B.9}$$

As the path length to reach the adjacent zone is $(\Delta x - x)/\mu$, photons born at $x < \Delta x - c\mu(\Delta t - t)$ do not have time to reach the adjacent zone. The energy that escapes into the adjacent zone is

$$4\pi \int_0^1 d\mu \int_0^{\Delta t} dt \int_{\Delta x - c\mu(\Delta t - t)}^{\Delta x} dx A e^{-\sigma(\Delta x - x)/\mu} \approx 2\pi A \Delta t \Delta x \varepsilon_x \left(1 - \varepsilon_t\right) \quad . \tag{B.10}$$

The holdover in the adjacent zone is

$$4\pi \int_0^1 d\mu \int_0^{\Delta t} dt \int_{\Delta x - c\mu(\Delta t - t)}^{\Delta x} dx A e^{-\sigma c(\Delta t - t)} \approx 2\pi A \Delta t \Delta x \varepsilon_t \varepsilon_x \quad . \tag{B.11}$$

The energy absorbed in the adjacent zone is obtained by subtracting the holdover, Eq. (B.11), from the energy that escapes into the zone, Eq. (B.10).

$$2\pi A \Delta t \Delta x \varepsilon_x \left(1 - 2\varepsilon_t\right) \tag{B.12}$$

The holdover energy in the birth zone is obtained by subtracting the holdover in the adjacent zone, Eq. (B.11), from the total holdover, Eq. (B.9).

$$2\pi A \Delta t \Delta x \varepsilon_t \left(2 - \varepsilon_x\right) \tag{B.13}$$

The energy absorbed in the birth zone is obtained by subtracting the energy that escaped into the adjacent zone, Eq. (B.10), and the holdover energy in the birth zone, Eq. (B.13), from the total energy emitted, Eq. (B.8).

$$2\pi A \Delta t \Delta x \left(2 - 2\varepsilon_t - \varepsilon_x + 2\varepsilon_t \varepsilon_x\right) \tag{B.14}$$

B.3 Interpolated derivative source of strength $A\mu$.

The configuration of this source term is shown in Fig. B.2. There are four half zones, each with a strength of $A\mu$, or $-A\mu$, as the case may be. We will assemble the energy deposition and holdover by considering two cases, a half zone just upstream of a zone boundary, and a half zone just downstream of

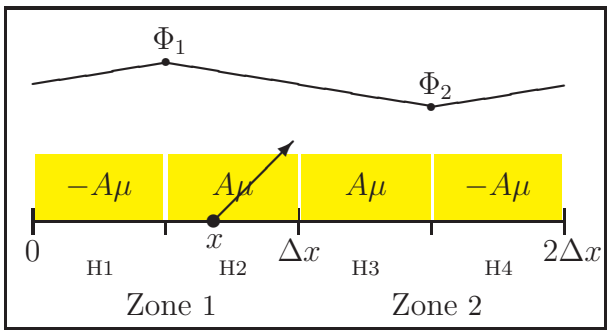

Fig. B.2. A depiction of the derivative source obtained by interpolating between zone centered values of Φ for the purpose of calculating the derivative, leading to a constant source strength of $A\mu$, or $-A\mu$, in half zones, as the case may be. The entire problem is shown, but we divide the problem domain into half zones in order to exploit symmetry when assembling the result. The labeled yellow regions mark the constant source in a given half zone, indicating the sign. A Monte Carlo particle born at position x in the half zone, H2, traveling in the direction shown by the arrow, travels a distance $s = (\Delta x - x)/\mu$ before escaping into the adjacent zone. A similarly directed Monte Carlo particle born in the half zone, H3, just to the right of the interface between zones is fully absorbed before it reaches the next zone.

a zone boundary, and then assemble the energy deposition and the holdover energy by considering the symmetries involved with the periodic boundary conditions.

The right moving energy emitted from a half zone of source strength $A\mu$ is

$$2\pi \int_0^1 d\mu \int_0^{\Delta t} dt \int_0^{\Delta x/2} dx A\mu = \frac{1}{2}\pi A \Delta t \Delta x \quad , \tag{B.15}$$

while the left moving energy from the same source has the opposite sign. The total holdover of this right moving emitted energy, without regard for the zone that it is in, is

$$2\pi \int_0^1 d\mu \int_0^{\Delta t} dt \int_0^{\Delta x/2} dx A\mu e^{-c\sigma(\Delta t - t)} \approx \frac{1}{2}\pi A \Delta t \Delta x \varepsilon_t \quad . \tag{B.16}$$

Specializing to a half zone just upstream of an interface between zones, the energy that crosses through the zone interface is

$$2\pi \int_0^1 d\mu \int_0^{\Delta t} dt \int_{\frac{1}{2}\Delta x - c\mu(\Delta t - t)}^{\frac{1}{2}\Delta x} dx A\mu e^{-\sigma(\frac{1}{2}\Delta x - x)/\mu} \approx \frac{2}{3}\pi A \Delta t \Delta x \varepsilon_x (1 - \varepsilon_t) \quad . \tag{B.17}$$

The holdover from the energy that crosses the interface between zones is

$$2\pi \int_0^1 d\mu \int_0^{\Delta t} dt \int_{\frac{1}{2}\Delta x - c\mu(\Delta t - t)}^{\frac{1}{2}\Delta x} dx A\mu e^{-c\sigma(\Delta t - t)} \approx \frac{2}{3}\pi A \Delta t \Delta x \varepsilon_t \varepsilon_x \quad . \tag{B.18}$$

The energy absorbed from an adjacent upstream half zone is given by sub-

tracting the holdover energy, Eq. (B.18), from the energy that crossed into the zone, Eq. (B.17),

$$\frac{2}{3}\pi A\Delta t\Delta x\varepsilon_x(1-2\varepsilon_t) \quad . \tag{B.19}$$

The holdover in the birth zone is obtained by subtracting the holdover from the energy that crossed the interface between zones, Eq. (B.18), from the total holdover, Eq. (B.16),

$$\pi A\Delta t\Delta x\varepsilon_t\left(\frac{1}{2}-\frac{2}{3}\varepsilon_x\right) \quad . \tag{B.20}$$

The energy absorbed in the birth zone is obtained by subtracting the energy that passed through the zone interface, Eq. (B.17), and the holdover in the birth zone, Eq. (B.20), from the energy emitted, Eq. (B.15),

$$\pi A\Delta t\Delta x\left(\frac{1}{2}-\frac{1}{2}\varepsilon_t-\frac{2}{3}\varepsilon_x+\frac{4}{3}\varepsilon_t\varepsilon_x\right) \quad . \tag{B.21}$$

Considering a half zone just downstream of an interface between zones, no Monte Carlo particles make it through the next half zone and therefore into the next zone, because they pick up a factor $e^{-\sigma\Delta x/\mu}\approx 0$. In this case the total holdover is restricted to the birth zone and, therefore, Eq. (B.16) becomes the holdover in the birth zone,

$$\frac{1}{2}\pi A\Delta t\Delta x\varepsilon_t \quad . \tag{B.22}$$

The energy absorbed in the birth zone is is the energy emitted, Eq. (B.15), minus the holdover, Eq. (B.16),

$$\frac{1}{2}\pi A\Delta t\Delta x(1-\varepsilon_t) \quad . \tag{B.23}$$

We now have, for a half zone just upstream of an interface between zones: the downstream energy absorbed in the birth zone, Eq. (B.21), the holdover in the birth zone, Eq. (B.20), the energy absorbed in the adjacent zone, Eq. (B.19), and the holdover in the adjacent zone, Eq. (B.18). For a half zone just downstream of an interface between zones: the energy absorbed in the birth zone is Eq. (B.23), while the holdover energy in the birth zone is Eq. (B.22). Returning to Fig. B.2, we can now tabulate the energy depositions to zone 1, progressing from H1 to H4 for right moving, and then the left moving, depositions, respectively. Each term is shown in Table B.1. The total energy deposition in zone 1 is the sum of these terms.

$$\frac{8}{3}\pi A\Delta t\Delta x\varepsilon_x(2\varepsilon_t-1) \tag{B.24}$$

Similarly, we tabulate the holdover energy in zone 1 due to the sources in each half zone in Table B.2. The total holdover energy in zone 1 is the sum of these

	H1	H2	H3	H4
right	-(B.23)	(B.21)	0	-(B.19)
left	(B.21)	-(B.23)	-(B.19)	0

Table B.1
The contributions to the energy deposition in zone 1 due to the source in each half zone, as arranged in Fig. B.2. The sign in the table entry is the sign of the contribution to the energy deposition, relative to the sign of the indicated expression. The rows labeled right and left are due to the right moving, and left moving sources, respectively.

	H1	H2	H3	H4
right	-(B.22)	(B.20)	0	-(B.18)
left	(B.20)	-(B.22)	-(B.18)	0

Table B.2
The contributions to the holdover energy in zone 1 due to the source in each half zone, as arranged in Fig. B.2. The sign in the table entry is the sign of the contribution to the holdover energy, relative to the sign of the indicated expression. The rows labeled right and left are the contributions due to right moving, and left moving sources, respectively.

terms.

$$-\frac{8}{3}\pi A\Delta t\Delta x\varepsilon_t\varepsilon_x \tag{B.25}$$

Considering the periodic boundary conditions, the absorbed energy and the holdover energy in zone 2 has the opposite sign.

References

[1] J.I. Castor, Radiation Hydrodynamics, Cambridge University Press, 2004.

[2] E. Larsen, The asymptotic diffusion limit of discretized transport problems, *Nucl. Sci. and Eng.*, 112:336–346, 1992.

[3] D. Knoll, J. Morel, L. Margolin, and M. Shashkov, Physically motivated discretization methods, *Los Alamos Science*, 29:188–212, 2005.

[4] J.E. Morel, T.A. Wareing, and K. Smith, A linear-discontinuous spatial differencing scheme for s_n radiative transfer calculations, *J. Comp. Phys.*, 128:445–462, 1996.

[5] T.C. Luu, E.D. Brooks III, and A. Szoke, Source tilting in the difference formulation for radiation transport, *Lawrence Livermore National Laboratory*, UCRL-JRNL-225197, 2006.

[6] A. Szoke and E.D. Brooks III, The transport equation in optically thick media, *J. Quant. Spect. Rad. Tran.*, 91:95, 2005.

[7] E.D. Brooks III, M.S. McKinley, F. Daffin, and A. Szoke, Symbolic implicit Monte Carlo radiation transport in the difference formulation: a piecewise constant discretization, *J. Comp. Phys.*, 205:737–754, 2005.

[8] E.D. Brooks III, A. Szoke, and J.D.L. Peterson, Piecewise linear discretization of symbolic implicit Monte Carlo radiation transport in the difference formulation, *J. Comp. Phys.*, 220:471-497, 2006.

[9] R.P. Smedley-Stevenson, Improved implicit Monte Carlo schemes based on the difference formulation, *Joint international topical meeting on mathematics and computation and supercomputing in nuclear applications (M&C + SNA 2007), Monterey, California, April 15-19, 2007, on CD-ROM, American Nuclear Society, LaGrange Park, IL (2007)*, 2007.

[10] E.D Brooks III, Symbolic implicit Monte Carlo, *J. Comp. Phys.*, 82:433–446, 1986.

[11] D. Mihalas and B. Weibel-Mihalas, *Foundations of Radiation Hydrodynamics*, Dover Publications, 1984.

[12] Y.B. Zel'dovich and Y.P. Raizer, *Physics of Shock Waves and High-Temperature Hydrodynamic Phenomena*, Dover Publications, 1966.